PNAS

# Supplementary Information

## ISL1 is necessary for auditory neuron development and contributes towards tonotopic organization

**Authors:** Iva Filova[a,1], Kateryna Pysanenko[b,1], Mitra Tavakoli[a], Simona Vochyanova[a], Martina Dvorakova[a], Romana Bohuslavova[a], Ondrej Smolik[a], Valeria Fabriciova[a], Petra Hrabalova[a], Sarka Benesova[c], Lukas Valihrach[c], Jiri Cerny[d], Ebenezer N. Yamoah[e], Josef Syka[b], Bernd Fritzsch[f*], and Gabriela Pavlinkova[a*]

**Affiliations:**
[a]Laboratory of Molecular Pathogenetics, Institute of Biotechnology CAS, 25250 Vestec, Czechia
[b]Department of Auditory Neuroscience, Institute of Experimental Medicine CAS, 14220 Prague, Czechia
[c]Laboratory of Gene Expression, Institute of Biotechnology CAS, 25250 Vestec, Czechia
[d]Laboratory of Light Microscopy, Institute of Molecular Genetics CAS, 14220 Prague, Czechia
[e]Department of Physiology, School of Medicine, University of Nevada Reno, NV 89557, USA
[f]Department of Biology, Department of Otolaryngology, University of Iowa, Iowa City, IA 52242-1324, USA
[1]These authors contributed equally: Iva Filova, Kateryna Pysanenko.
[*] Email: bernd-fritzsch@uiowa.edu and Gabriela.Pavlinkova@ibt.cas.cz

**This PDF file includes:**
SI Materials and Methods
Figures S1 to S10
Tables S1 to S2
Legends for Movies S1 to S4

**Other supplementary materials for this manuscript include the following:**

Movies S1 to S4
Datasets S1 to S2

## Materials and Methods

### Experimental animals

All experiments involving animals were performed according to the Guide for the Care and Use of Laboratory Animals (National Research Council. Washington, DC. The National Academies Press, 1996). The design of experiments was approved by the Animal Care and Use Committee of the Institute of Molecular Genetics, Czech Academy of Sciences (protocol # 104/2019). The mice were housed in 12-hour light/dark cycles and were fed *ad libitum*. To generate *Isl1CKO* (the genotype *Neurod1$^{Cre}$;Isl1$^{loxP/loxP}$*), we cross-bred floxed *Isl1* (*Isl1$^{loxP/loxP}$*; *Isl1$^{tm2Sev}$/J*, # 028501, Jackson Laboratory)[25] and *Neurod1$^{Cre}$* transgenic mice (Tg(Neurod1-cre)1Able/J, # 028364, Jackson Laboratory), which were generated by pronuclear injection of the *Neurod1-cre* BAC construct that carries Cre-sequence downstream of the translational initiation codon ATG of the *Neurod1* gene [24]. Heterozygous animals, *Neurod1$^{Cre}$;Isl1$^{+/loxP}$* were viable, born in appropriate Mendelian ratios, and were phenotypically indistinguishable from control (Cre negative) littermate mice. As control mice, we used mice with the genotype Cre negative, *Isl1$^{loxP/loxP}$*, and *Isl1$^{+/loxP}$*. The mouse line *Neurod1$^{Cre}$* was also bred with Cre-reporter tdTomato line (*TomatoAi14*, B6.Cg-*Gt(ROSA)26Sor$^{tm14(CAG-tdTomato)Hze}$*, # 7914 Jackson Laboratory). Using tdTomato reporter for our analyses, we compared the reporter control-*Ai14* (genotype: *Neurod1$^{Cre}$;Isl1$^{+/loxP}$;TomatoAi14*) and reporter *Isl1CKO-Ai14* (genotype: *Neurod1$^{Cre}$;Isl1$^{loxP/loxP}$;TomatoAi14*). We performed PCR genotyping on tail DNA. We used both males and females for experiments. Lines are a mixed C57BL/6/sv129 background. Phenotyping and data analyses were performed blind to the genotype of the mice.

### Morphological evaluation of the cochlea, the CN, and the IC

Dissected ears were fixed in 4% paraformaldehyde (PFA) in PBS. For vibratome sections, samples were embedded in 4% agarose and sectioned at 80 μm using a Leica VT1000S vibratome. Vibratome sections, whole inner ears, or whole embryos were defatted in 70% ethanol and then rehydrated and blocked with serum, as described previously [1, 2]. Samples were then incubated with primary antibodies at 4ºC for 72 hours. The primary antibodies used were: rabbit anti-Myosin 7a (Myo7a; Proteus BioSciences 25-6790, 1:500), mouse anti-acetylated α-tubulin (tubulin; Sigma-Aldrich T6793, 1:400), rabbit anti-calretinin (Santa Cruz Biotechnology sc-50453, 1:100), goat anti-prestin (Santa Cruz Biotechnology sc-22692, 1:50), rabbit anti-parvalbumin (Abcam ab11427, 1:2000), mouse anti-VGLUT1 (Merck MAB5502, 1:200), rabbit anti-NeuN (Abcam ab177487, 1:500), mouse anti-Isl1 (Developmental Hybridoma Bank 39.3F7 or 39.4D5, 1:130), mouse anti-C-terminal binding protein 2 (CtBP2; BD Biosciences 612044, 1:200), rabbit anti-cleaved Caspase-3 (Cell Signaling Technology 9661, 1:100), goat anti-Neurod1 (Santa Cruz Biotechnology sc-1084, 1:100), anti-β tubulin III (Tuj1; BioLegend 801202, 1:500), and rabbit anti-Sox10 (Abcam ab155279, 1:250). After several PBS washes, secondary antibodies were added and incubated at 4ºC for 24 hours. The secondary antibodies Alexa Fluor® 488 AffiniPure Goat Anti-Mouse IgG (Jackson ImmunoResearch Laboratories 115-545-146), Alexa Fluor® 594 AffiniPure Goat Anti-Rabbit IgG (Jackson ImmunoResearch Laboratories 111-585-144), DyLight488-conjugated AffiniPure Mouse Anti-Goat IgG (Jackson ImmunoResearch Laboratories 205-485-108), Alexa Fluor® 647-conjugated AffiniPure Donkey Anti-Goat IgG (Jackson ImmunoResearch Laboratories 705-605-147), Alexa Fluor® 594-conjugated AffiniPure Donkey Anti-Rabbit IgG (Jackson ImmunoResearch Laboratories 711-585-152), and Alexa Fluor®488-conjugated AffiniPure Donkey Anti-Mouse IgG (Jackson ImmunoResearch Laboratories 715-545-150) were used in 1:400 dilution. Nuclei were stained by Hoechst 33258 (Sigma-Aldrich 861405, 1:2000). Samples were mounted in Aqua-Poly/Mount (Polysciences 18606) or prepared

Antifade medium. Images were taken on Zeiss LSM 880 NLO inverted confocal microscope, Nikon CSU-W1 spinning disk confocal microscope, and Carl Zeiss AxioZoomV16 macroscope. NIS-Elements, ImageJ, and ZEN software were used for image processing.

The length of the organ of Corti was measured using the "Measure line" ImageJ plugin. The volumes of the CN and IC were established by analyzing parallel, serial, equally spaced 80 µm coronal vibratome sections through the brain (n = 5 *Isl1CKO* and n = 5 control mice). The CN and IC areas were determined in each section using ImageJ, and the volume of the organs was calculated. Volumes of organs were adjusted to the body weight. Whole-mount anti-tubulin labeling of the cochlea was used to measure the length and density of the radial fibers. The evaluation of the innervation was done separately for each region of the cochlea: the apex, mid-apex, mid-base, and base. Due to the disorganization of innervation in the apex, we only evaluated the cochlear base, mid-base, and mid-apex fiber density. The density of the radial fibers was expressed as the percentage of a positive area in the measured area of 152 x 66 $\mu m^2$ using the "Threshold" function of ImageJ. The length of the radial fibers was measured from the whole-mount anti-tubulin and Myo7a immunolabeled cochlea confocal images. For each genotype, we measured 3 samples, and in all four regions of the cochlea (the apex, mid-apex, mid-base, and base), we measured the length of the fibers in 3 radial fiber bundles from the IHCs to the IGSB. To compare how many neurons are correctly located in the Rosenthal's canal in *Isl1CKO*, we used NeuN immunolabeled whole-mount cochlea (n = 4 per genotype). Cells were manually counted in 40x magnification images in 5 Z-stacks using the "Cell counter" function of ImageJ; the area of the Rosenthal's canal with tdTomato$^+$ neurons was measured using "Threshold", "Polygon selection" and "Measure" functions of ImageJ to calculate the relative number of neurons for the control and *Isl1CKO* per Rosenthal's canal volume. For ribbon evaluations, IHCs were counted based on the calretinin-stained cell bodies and anti-CtBP2 labeled synapses. CtBP2$^+$ presynaptic ribbon structures were manually counted in 10 individual IHCs in each cochlear region: the apex, mid-apex, mid-base, and base. A total of 6 mutants and 6 control cochleae were evaluated except for 1 apex in the control group, which was lost during immunolabeling. The apoptosis of neurons was quantified using immunohistochemistry with anti-cleaved Caspase-3. Caspase-3 positive cells were manually counted in the inner ear ganglia labeled by the combination of anti-Cre and anti-Neurod1 in the whole-mounted head at 60x magnification at E10.5. For E12.5, Caspase-3$^+$/tdTomato$^+$ neurons were manually counted in the whole-mounted inner ear at 60x magnification. The area of E12.5 inner ear ganglia was measured using the "Threshold and polygon selection" function of ImageJ. For E14.5, the cochlea was sectioned, and Caspase-3$^+$/tdTomato$^+$ neurons were manually counted in all sections at 60x magnification. Three embryos per genotype were used for each embryonic day. All apoptotic cell counting was done using the "Cell counter" function of ImageJ. The density of spherical bushy cells in the VCN, 3 control and 3 *ISL1CKO* 2-month-old mice were used. Bushy cells were labeled by anti-parvalbumin in 80 µm vibratome sections, and manually counted in 2-4 sections/animal in 134.95 x 134.95 µm (63x objective). The size of vestibular sensory epithelia was measured in anti-Myo7a labeled wholemount preparations at P0. Myo7a$^+$ areas were measured in 5 control and 5 *Isl1CKO* mice using "Measure" ImageJ tool. The dorsal root ganglia (DRG) size was evaluated in the sagittal sections of E14.5 embryos with expression of tdTomato reporter. The area of DRG was quantified in 6 embryos per genotype and 2 sections per embryo using the "Threshold and polygon selection" function of ImageJ.

**Light-sheet fluorescent microscopy (LFSM) and analysis of images**

The cochleae were microdissected from 2 control-*Ai14* and 2 *Isl1CKO-Ai14* mice (postnatal day P0). We used an advanced CUBIC protocol[3] for tissue clearing to enable efficient imaging by light-sheet microscopy. Briefly, the microdissected cochlea was fixed in 4% PFA for 1 hrs,

washed with PBS, and incubated in a clearing solution Cubic 1 for 7 days at 37ºC. Before immunolabeling, samples were washed in PBT (0.5% Triton-X in PBS) 4 x for 30 min. In addition to *tdTomato* expression, cochlear samples were either immunolabeled using anti-NeuN (a nuclear marker of differentiated neurons) or anti-Myo7a (a hair cell marker) antibodies. Samples were stored before imaging in Cubic 2 at room temperature. Zeiss Lightsheet Z.1 microscope with illumination objective Lightsheet Z.1 5x/0.1 and detection objective Dry objective Lightsheet Z.1 5x/0.16 was used for imaging at the Light Microscopy Core Facility of the Institute of Molecular Genetics of the Czech Academy of Sciences. IMARIS software v8.1.1 (Bitplane AG, CA, USA) was used for image processing.

**Isolation of genetically labeled neurons and library construction**

Spiral ganglia were micro-dissected in Dulbecco's PBS on ice from E14.5 embryos of either sex from four litters; each sample contains spiral ganglia from both inner ears of the individual embryo. Spiral ganglia were incubated in 300 µl of lysis solution (0.05% trypsin, 0.53mM EDTA in Dulbecco's PBS) in 37 ºC, shaking at 900 RPM for 5 min. The lysis was stopped by adding 600 µl of FACS buffer (10mM EGTA, and 2% FBS in Dulbecco's PBS). After spinning down the samples at 800 G, 4 ºC for 10 min, the supernatant was removed, and cell pellets were resuspended in 500 µl of ice-cold FACS buffer. Immediately before sorting, cells were passed through a 50 µm cell sieve (CellTrics™, Sysmex Amercica Inc.) into a sterile 5 ml polystyrene round-bottom falcon to remove clusters of cells and kept on ice. TdTomato$^+$ neurons were sorted using a flow cytometer (BD FACSAria™ Fusion), through a 100 µm nozzle in 20 psi, operated with BD FACSDiva™ Software (Fig. S10). 100 sorted cells were collected into individual wells of 96-well plate containing 5 µl of lysis buffer of NEB Next single-cell low input RNA library prep kit for Illumina (New England Biolabs #E6420). Plates were frozen immediately on dry ice and stored at −80 °C. The total time from euthanasia to cell collection was ~3 hrs.

RNAseq-libraries were prepared from 6 samples per each genotype, reporter control-*Ai14* and *Isl1CKO-Ai14* mutant, and each sample contained 100 tdTomato$^+$ neurons. Following the manufacturer's instructions, the NEB Next single-cell low input RNA library prep kit for Illumina was used for cDNA synthesis, amplification, and library generation [4] at the Gene Core Facility (Institute of Biotechnology CAS, Czechia). Fragment Analyzer assessed the quality of cDNA libraries. The libraries were sequenced on an Illumina NextSeq 500 next-generation sequencer. NextSeq 500/550 High Output kit 75 cycles (Illumina #200024906) were processed at the Genomics and Bioinformatics Core Facility (Institute of Molecular Genetics CAS, Czechia).

**Computational analysis of RNAseq data**

RNA-Seq reads in FASTQ files were mapped to the mouse genome using STAR [version 2.7.0c [5]] GRCm38 primary assembly and annotation version M8. The raw data of RNA sequencing were processed with a standard pipeline. Using cutadapt v1.18[6], the number of reads (minimum, 32 million; maximum, 73 million) was trimmed by Illumina sequencing adaptor and of bases with reading quality lower than 20, subsequently reads shorter than 20 bp were filtered out. TrimmomaticPE version 0.36 [7]. Ribosomal RNA and reads mapping to UniVec database were filtered out using bowtie v1.2.2. with parameters -S -n 1 and SortMeRNA [8]. A count table was generated by Rsubread v2.0.1 package using default parameters without counting multi mapping reads. The raw RNAseq data were deposited at GEO: # GSE182575 study (https://www.ncbi.nlm.nih.gov/geo/query/acc.cgi?acc=GSE182575). DESeq2 [v1.26.0 [9]] default parameters were used to normalize data and compare the different groups. Differentially expressed genes were identified based on an adjusted P-value $p_{adj} < 0.05$, FC > 2, and a base mean ≥ 50 was applied to identify differentially expressed genes

between *Isl1CKO* mutant and control neurons. The functional annotation of the differentially expressed genes was performed using GOTermFinder [10].
*Enrichment mapping*. The enrichment of the functional categories and functional annotation clustering of the differentially expressed genes was performed using g: Profiler [11] input using version e104_eg51_p15_3922dba with g: SCS multiple testing correction methods applying a significance threshold of 0.05. In contrast, no electronic GO annotations were used. Only Biological Processes (BP) data underwent further processing. Complete query details are available in Query info tabs in Dataset S2. The resulting GEM and combined GMT files were loaded into Cytoscape [12] plugin "EnrichmentMap" [13] using 0.01 FDR q-value cutoff to generate a network. Edge cutoff was set to 0.6, and nodes were filtered by gs_size<1800. Five GO terms forming solitary nodes, or a pair of nodes, were excluded (listed in Dataset S2). Further adjustments were made in yFiles Layout Algorithms, Legend Creator (Cytoscape plugins), and Inkscape (Inkscape Project, 2020).

**Quantitative real-time PCR**
Total RNA was isolated from both inner ears of the embryo at E14.5 using TRI Reagent (Sigma-Aldrich T9424). We used 8 embryos for *Isl1CKO* and 7 embryos for the control group from three litters. RNA from both inner ears of one embryo represented one sample. RNA samples (0.5 μg of total RNA) were processed and analyzed as previously described [2, 14]. Briefly, following RT, quantitative qPCR was performed with initial activation at 95 °C for 120 s, followed by 40 cycles at 95 °C for 15 s, 60 °C for 30 s, and 72 °C for 30 s using the CFX384™ Real-Time PCR Detection System (Bio-Rad Laboratories). The primer sequences (*Lhx1, Lhx2, Cdh7, Nhlh2, Ntrk2, Ntrk3, Ntng1*) were obtained from (pga.mgh.harvard.edu/primerbank/) or designed using Primer3 tool (*Dcc, Epha5, Gata3, Prdm8, Robo2, Slit2, Tbx3, Uncx*). The primer sequences are listed in Table S2. Relative mRNA expression was calculated using the –ΔΔCq method with *Hprt1* as a reference gene. GraphPad Prism software was used for statistical analysis.

**Lipophilic Dye Tracing**
We studied the innervation pattern in whole or dissected ears using lipophilic dye tracing in aldehyde-fixed tissues as previously described [15]. At least three mutants and similar numbers of control littermates of both sexes were used for each evaluation. Filter strips loaded with NeuroVue colored lipophilic dyes were inserted into the cochlear apex, base, and vestibular end-organ utricle. After allowing appropriate time for diffusion of the lipophilic tracer (between 48-120 hours), we prepared the ears as whole mounts in glycerol on a glass slide, using appropriate spacers to avoid distortion, and imaged them using a Leica SP8 confocal microscope. Images were compiled into plates to show the most pertinent details using Corel Draw. Only general image modifications such as contrast, or brightness adjustments were used to enhance the visual appeal without affecting the scientific content.

**Hearing function evaluation**
Auditory brainstem response (ABR) and distortion product otoacoustic emissions (DPOAEs) tests were carried out on mice under general anesthesia with 35 mg/kg ketamine (Calypso 50 mg/ml) and 6 mg/kg xylazine (Xylapan 20 mg/ml) in saline to give an application volume of 7 ml/kg body weight via subcutaneous injection, maintained on a temperature-regulated blanket in a soundproof room.
*Distortion product otoacoustic emissions.* For DPOAE recording were tested *Isl1CKO* (n = 10) and control mice (n = 14). Cubic (2 F1–F2) distortion product otoacoustic emissions over an F2 frequency range from 4 to 39 kHz were recorded with a low-noise microphone system (Etymotic probe ER-10B+, Etymotic Research). Acoustic stimuli (ratio F2/F1 = 1.21, F1 and

F2 primary tone levels of L1/L2 = 70/60 dB) were presented to the ear canal with two custom-made piezoelectric stimulators connected to the probe with 10-cm-long silastic tubes. The signal from the microphone was analyzed by the TDT System III (RP2 processor, sampling rate 100 kHz) using custom-made MATLAB software. DPOAEs were recorded in the animals' ears at individual frequencies over the frequency range 4–39 kHz with a resolution of ten points per octave. All the experiments and analyses were done with no information on the genotype.
*Auditory brainstem response.* For auditory brainstem response (ABR) recording (n = 10 *Isl1CKO* and n = 11 control mice), an active electrode was placed subcutaneously on the vertex and ground and reference electrodes in the neck muscles. Responses to tone bursts (3 ms duration, 1 ms rise/fall times, frequencies of 2, 4, 8, 16, 32, and 40 kHz) and clicks of different intensity were recorded. Acoustic stimuli were conveyed to the animal in free-field conditions via a two-way loudspeaker system (Selenium 6W4P woofer and RAAL70-20 tweeter) placed 70 cm in front of the animal's head. The signal was processed with a TDT System III Pentusa Base Station and analyzed using BioSig™ software. The response threshold to each frequency was determined as the minimal tone intensity that still evoked a noticeable potential peak in the expected time window of the recorded signal. The amplitude and latency of ABR peaks I-V were determined using BioSig software (Tucker Davis Technologies). Central compensation of neuronal responsiveness (central gain) was calculated using ABR wave IV to I amplitudes.

**Extracellular recording of the neuronal activity in the IC**
For extracellular recording in the IC, we evaluated *Isl1CKO* (n = 12, 624 units) and control mice (n = 8, 395 units). The surgery and extracellular recording in the IC were performed in mice anesthetized with 35 mg/kg ketamine (Calypsol 50 mg/ml) and 6 mg/kg xylazine (Xylapan 20 mg/ml) in saline via subcutaneous injection. Approximately every hour, supplement subcutaneous injections of one-half of the original dose of the anesthetics were administered to keep a sufficient level of anesthesia, judged by a positive pedal and palpebral (toe-pinch) reflex and movement of the whiskers. Respiratory rate, and heart rate, were monitored. An incision was made through the skull's skin to access the IC, and underlying muscles were retracted to expose the dorsal skull. A holder was glued to the skull, and small holes were drilled over both ICs. Neuronal activity (multiple units) in the IC was recorded using a 16-channel, single shank probe (NeuroNexus Technologies) with 50 or 100 μm between the electrode spots. The obtained signal from the electrode was amplified 10000 times, band-pass filtered over the range of 300 Hz to 10 kHz, and processed by a TDT System III (Tucker Davis Technologies) using an RX5-2 Pentusa Base Station. Individual spikes from the recorded signal were isolated online based on amplitude discrimination and analyzed with BrainWare software (v. 8.12, Jan Schnupp, Oxford University). Subsequent discrimination of spikes from the recorded data and their sorting according to the amplitudes of the first positive and negative peaks were performed off-line and was used to sort action potentials (spikes) among single units. The recorded data were processed and analyzed using custom software based on MATLAB. The stimulation signals were generated using a TDT System III with the RP 2.1 Enhanced Real-Time Processor. Acoustic stimuli were delivered in free-field conditions via a two-driver loudspeaker system (Selenium 6W4P woofer and RAAL70-20 tweeter) placed 70 cm in front of the animal's head.
*Frequency-intensity mapping:* To determine the neuronal receptive fields, pure tones (frequency 2 - 40 kHz with 1/8 octave step, 60 ms duration, 5 ms rise/fall times, various intensity with 5dB step) were presented in a random order, each stimulus appearing three times. A discrete matrix corresponding to the response magnitude evoked by each of the frequency-intensity combinations was thereby obtained, smoothed using cubic spline interpolation, and used for extraction of the basic parameters: the excitatory response threshold (the lowest stimulus intensity that excited the neuron, measured in dB SPL), the characteristic frequency

(CF) – the frequency with the minimal response threshold, measured in Hz, and the bandwidth of the excitatory area 20 dB above the excitatory threshold, expressed by quality factor Q (Q = CF/bandwidth).
*Rate intensity function of the IC neurons:* Neuronal responses to broadband noise (BBN) bursts of variable intensity (10 dB steps, 50 repetitions) were used to construct the rate intensity function (RIF). A 100% scale was assigned to the neuron's total range of response amplitudes, 0% corresponding to spontaneous activity and 100% corresponding to its maximum response magnitude [16]. The two points of interest are R10 and R90, which correspond to 10 and 90% of this scale, respectively. R10, describing the starting point of the RIF's rise, was taken as the BBN response threshold. RIFs were further used to evaluate the following parameters: the dynamic range (DR) of the RIF: DR = S90–S10); and the maximum response magnitude. Spontaneous activity of the IC neurons was determined at the 0dB SPL BBN stimulation.
*Temporal properties of the IC neurons:* We used trains of five clicks at an intensity of 70 dB SPL for control and 80 dB SPL for *Isl1CKO* mice with various inter-click intervals (100, 50, 30, 20, and 15 ms). We calculated the vector strength (VS) values and the Rayleigh statistics for each spike pattern; only responses with at least 5.991 were significantly considered phase-locking (Zhou and Merzenich, 2008). The VS quantifies how well the individual spikes are synchronized (phase-locked) with a periodic signal.

**Behavioral tests of motor coordination and balance**
All testing was carried out during the light cycle and after a minimum 30-min acclimatization.
*Air-righting reflex.* The vestibular function was evaluated by the ability of the mice to right themselves in the air when held supine and dropped onto a soft surface from a height of 50 $cm^2$.
*Rotarod.* Using the rotarod apparatus (Rota Rod 47600, Ugo Basile), the time (latency) to fall off the rod rotating under continuous acceleration was recorded. During the acclimatization period, mice with their heads in the direction of rotation were loaded on the rotarod at an initial speed of 4 rpm. This speed was maintained for 2 min and, if mice fell during this period, they were placed back on the rotarod. The drum was slowly accelerated from 4 to 40 rpm for a maximum of 300 s for each trial for the experimental measurements. The latency to fall off the rotarod within 300 s was recorded. If the mouse clung to the grip of the rotating rod and failed to resume normal performance for three consecutive revolutions, the sensor was manually triggered. Mice were tested in three consecutive trials in one session per day with a 15-min rest period between each trial.

**Behavioral acoustic tests**
*Isl1CKO* (n = 10) and control (n = 7) mice were used at 2-3 months of age. All behavioral tests were performed in a sound-attenuated chamber (Coulbourn Habitest, model E10-21) located in a soundproof room. Each mouse was placed in a wire mesh cage on a motion-sensitive platform inside the box during the testing. The mouse's reflex movements to sound stimuli were detected and transformed to a voltage signal by the load-cell response sensing platform. An amplified voltage signal was acquired and processed using a TDT system 3 with a Real-Time Processor RP 2 (Tucker Davis Technologies, Alachua, Fl) and custom-made software in a Matlab environment. The startle responses were evaluated in 100 ms windows, beginning at the onset of the startling stimulus. The magnitude of the response was measured as the maximal peak-to-peak amplitude of transient voltage occurring in the response window. Acoustic stimuli were generated by the TDT system (Real-Time Processor RP 2), amplified and presented via a loudspeaker (SEAS, 29AF/W), and placed inside the chamber above the animal. Stimulus presentation and data acquisition were controlled by a custom-made application in a Matlab environment. Calibration of the apparatus was performed for frequencies between 4

kHz and 32 kHz by a 1/4-inch Brüel & Kjaer 4939 microphone connected to a Brüel & Kjaer ZC 0020 preamplifier and a B&K 2231 sound level meter. During the calibration, the calibrating microphone was positioned at the animal's head in the test cage.
*Acoustic startle reflex (ASR)* (a transient motor response to an intense, unexpected stimulus) was used to indicate the behavioral responsiveness to sound stimuli**.** The ASRs to 8, 16, and 32 kHz tone pips and BBN bursts (50 ms duration, 3 ms rise/fall times, varying intensity levels) were recorded. Each test session contained: a baseline trial (–10 dB SPL stimulus intensity) and 13 startle stimuli of different intensities (50, 55, 60, 65, 70, 75, 80, 85, 90, 100, 110, 115, and 120-dB SPL). The inter-trial interval varied from 15 to 50 s.
In *the prepulse inhibition (PPI)* procedure, 3 different trial types were used: a baseline trial without any stimulus, an acoustic startle pulse alone (white noise at 110 dB SPL, 50 ms, 3 ms rise/fall times), and a combination of the prepulse and startle pulse. The inter-stimulus interval between the prepulse and the startle stimulus was set to 50 ms; each trial type was presented three times. The inter-trial gap was randomized and varied from 15 to 50 s. The efficacy of the PPI of ASR was expressed as an ASR ratio in percentage, e.g., 100% corresponds to the amplitude of ASR without prepulse; smaller values of ASR ratio indicate stronger PPI. As a prepulse, we used either BBN bursts or tone pips (50 ms duration, 3 ms rise/fall time) at frequencies of 8 and 32 kHz at increasing intensities. It is expected that in the presence of prepulse, the amplitude of the following startle response decreases.

**Experimental design and statistical analyses**
All comparisons were made between animals with the same genetic background, typically littermates, and we used male and female mice. The number of samples (n) for each comparison can be found in the individual method descriptions and are given in the corresponding figures. Phenotyping and data analysis was performed blind to the genotype of the mice. All values are presented either as the mean ± standard deviation (SD) or standard error of the mean (SEM). For statistical analysis, GraphPad Prism software was used. To assess differences in the mean, one-way or two-way ANOVA with Bonferroni's multiple comparison test, multiple *t*-tests with Holm-Sidak comparison method, repeated measures ANOVA, multiple *t*-tests, and unpaired two-tailed *t*-tests were employed. Significance was determined as $P < 0.05$ (*), $P < 0.01$ (**), $P < 0.001$ (***) or $P < 0.0001$ (****). Complete results of the statistical analyses are included in the figure legends.

**References**


1. Dvorakova M, *et al.* Incomplete and delayed Sox2 deletion defines residual ear neurosensory development and maintenance. *Sci Rep* **6**, 38253 (2016).

2. Bohuslavova R, *et al.* Pax2-Islet1 Transgenic Mice Are Hyperactive and Have Altered Cerebellar Foliation. *Mol Neurobiol* **54**, 1352-1368 (2017).

3. Susaki EA, Tainaka K, Perrin D, Yukinaga H, Kuno A, Ueda HR. Advanced CUBIC protocols for whole-brain and whole-body clearing and imaging. *Nat Protoc* **10**, 1709-1727 (2015).

4. Mamanova L, Miao Z, Jinat A, Ellis P, Shirley L, Teichmann SA. High-throughput full-length single-cell RNA-seq automation. *Nat Protoc* **16**, 2886-2915 (2021).

5. Dobin A, *et al.* STAR: ultrafast universal RNA-seq aligner. *Bioinformatics* **29**, 15-21 (2013).

6. Martin M. Cutadapt removes adapter sequences from high-throughput sequencing reads. *2011* **17**, 3 (2011).

7. Bolger AM, Lohse M, Usadel B. Trimmomatic: a flexible trimmer for Illumina sequence data. *Bioinformatics* **30**, 2114-2120 (2014).

8. Kopylova E, Noe L, Touzet H. SortMeRNA: fast and accurate filtering of ribosomal RNAs in metatranscriptomic data. *Bioinformatics* **28**, 3211-3217 (2012).

9. Love MI, Huber W, Anders S. Moderated estimation of fold change and dispersion for RNA-seq data with DESeq2. *Genome Biol* **15**, 550 (2014).

10. Boyle EI, *et al.* GO::TermFinder--open source software for accessing Gene Ontology information and finding significantly enriched Gene Ontology terms associated with a list of genes. *Bioinformatics* **20**, 3710-3715 (2004).

11. Raudvere U, *et al.* g:Profiler: a web server for functional enrichment analysis and conversions of gene lists (2019 update). *Nucleic acids research* **47**, W191-W198 (2019).

12. Shannon P, *et al.* Cytoscape: a software environment for integrated models of biomolecular interaction networks. *Genome Res* **13**, 2498-2504 (2003).

13. Merico D, Isserlin R, Stueker O, Emili A, Bader GD. Enrichment map: a network-based method for gene-set enrichment visualization and interpretation. *PLoS One* **5**, e13984 (2010).

14. Filova I, *et al.* Combined Atoh1 and Neurod1 Deletion Reveals Autonomous Growth of Auditory Nerve Fibers. *Mol Neurobiol* **57**, 5307-5323 (2020).

15. Fritzsch B, Duncan JS, Kersigo J, Gray B, Elliott KL. Neuroanatomical Tracing Techniques in the Ear: History, State of the Art, and Future Developments. In: *B. Sokolowski, Ed: Auditory and Vestibular Research: Methods and Protocols*). Springer Science+Business Media New York (2016).

16. Bures Z, Grécová J, Popelár J, Syka J. Noise exposure during early development impairs the processing of sound intensity in adult rats. *The European journal of neuroscience* **32**, 155-164 (2010).

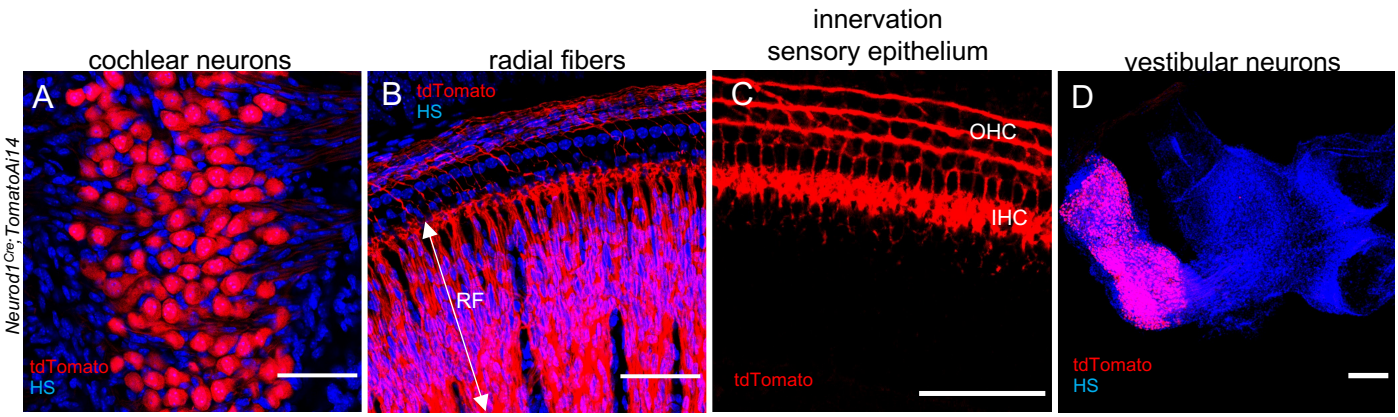


**Fig. S1. The expression pattern of *Neurod1*$^{Cre}$ shown by tdTomato reporter in the cochlea and vestibular ganglion of the *Neurod1-Cre;Ai14 tdTomato* mouse.** The confocal images from cochlear whole-mount preparations show in detail **(A)** tdTomato expression in neurons, **(B)** tdTomato$^{+}$ labeled neurites extending from neurons as radial fibers (RF) to the sensory cells, and **(C)** tdTomato$^{+}$ neurites formed three rows of outer spiral bundles beneath the outer hair cells (OHC) and the inner spiral plexus associated with the inner hair cells (IHC). **(D)** tdTomato$^{+}$ neurons of vestibular ganglion are shown in the whole-mount of the inner ear. HS, Hoechst nuclear staining. Scale bars: 50 μm (a-c), 200 μm (d).

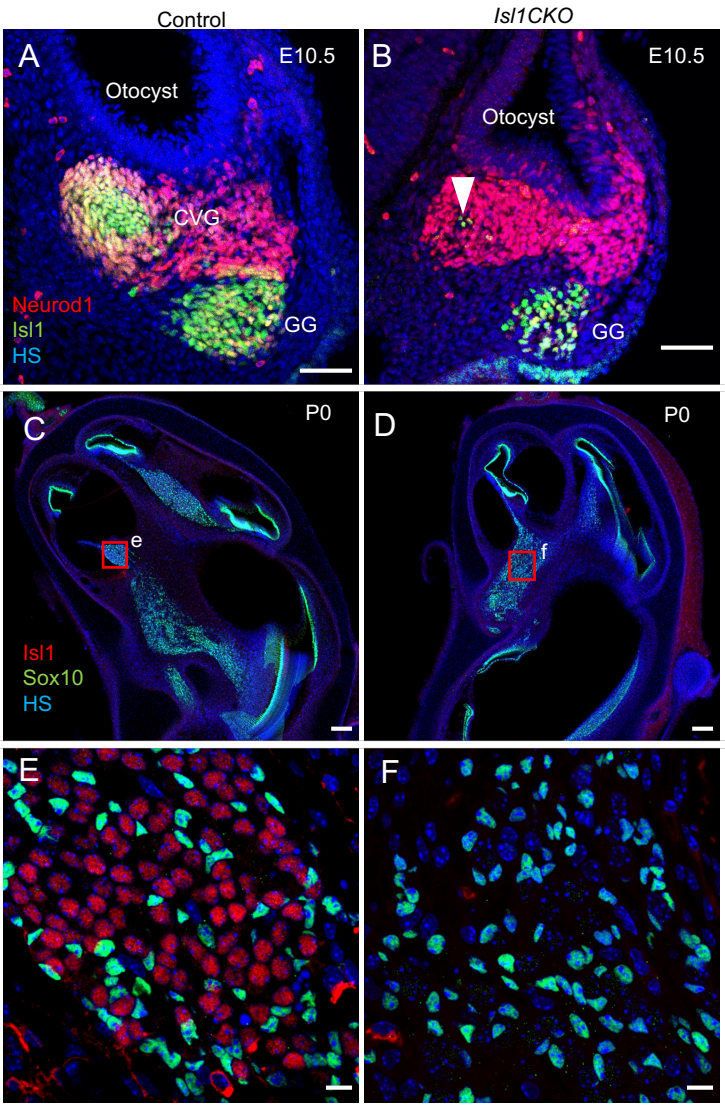


**Fig. S2. Elimination of ISL1 shown in inner ear neurons of *Isl1CKO*. (A, B)** In E10.5 control embryos, ISL1 is expressed in differentiating neurons of cochleovestibular ganglion (CVG) and geniculate ganglion (GG), whereas ISL1 is detected only in a few neurons in the CVG of *Isl1CKO* (arrowhead). **(C-F)** At P0, ISL1 is eliminated in spiral ganglion neurons of *Isl1CKO.* Note presence of glial cells in the spiral ganglion (Sox10 is a marker of glial cells). HS, Hoechst nuclear staining. Scale bars: 50 µm (A, B); 100 µm (C, D); 10 µm (E, F).

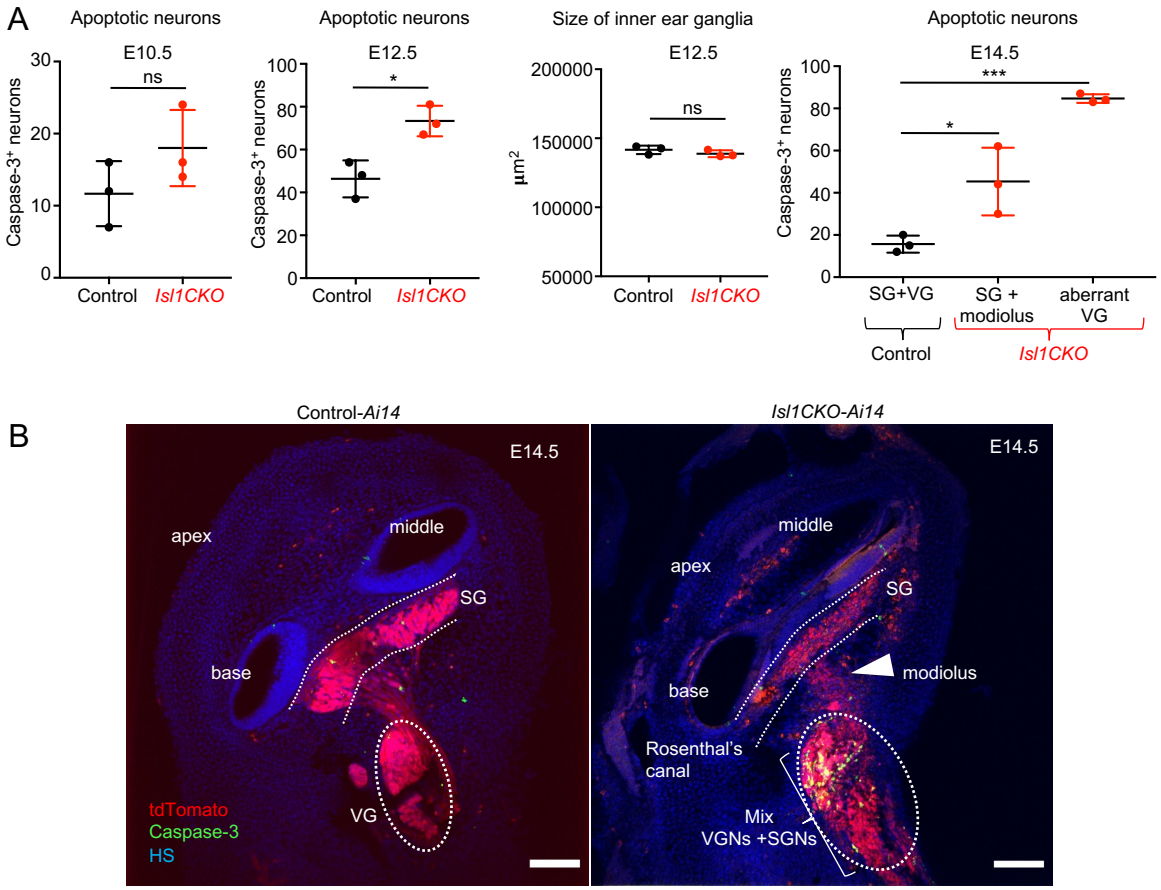


**Fig. S3. Quantification of apoptotic neurons in the developing inner ear. (A)** The number of apoptotic neurons was manually counted in inner ear ganglia at E10.5, E12.5 and E14.5 using immunolabeling with anti-cleaved Caspase-3. The size of E12.5 inner ear ganglia is comparable between control and mutant. At E14.5, the total number of apoptotic neurons were counted in the spiral and vestibular ganglia of control embryos. In *Isl1CKO,* apoptotic neurons were counted in all areas containing neurons: the Rosenthal's canal (spiral ganglion), modiolus, and the area outside of the cochlea corresponding to the region of the vestibular ganglion in controls. Error bars represent mean ± SD (n = 3 embryos per genotype); unpaired *t*-test (E10.5, E12.5), *P = 0.0158; ns, not significant; and one-way ANOVA followed by Dunnett's multiple comparisons test (E14.5), *P = 0.0284, ***P = 0.0002. **(B)** The representative sections of the inner ear of E14.5 embryos show tdTomato$^{+}$ neurons and immunolabeled apoptotic cells by anti-cleaved Caspase-3. HS, Hoechst nuclear staining; SG, spiral ganglion; SGNs, spiral ganglion neurons; VGNs, vestibular ganglion neurons; VG, vestibular ganglion. Scale bars: 100 µm.

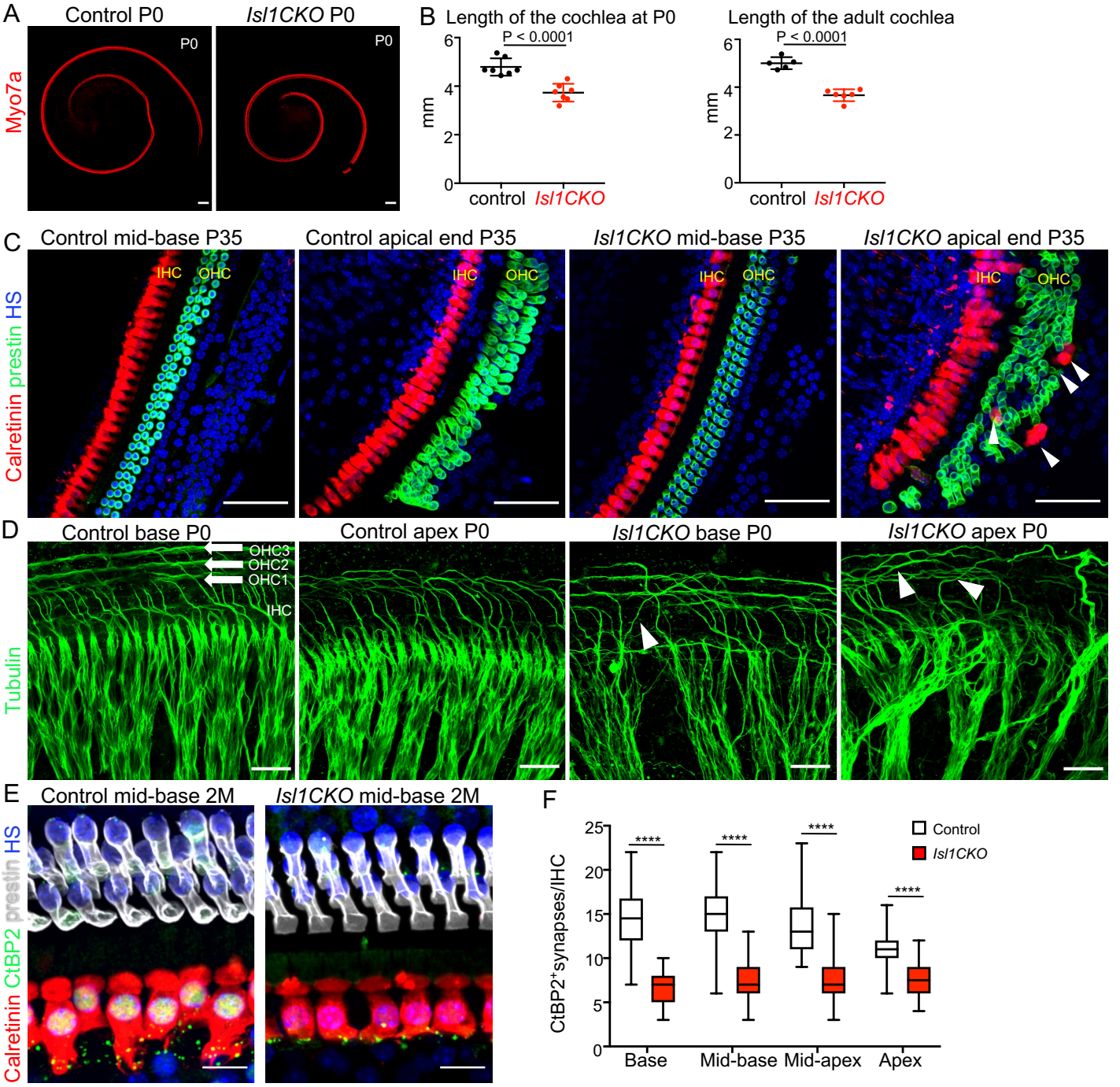


**Fig. S4.** The length of the organ of Corti is shortened, the apical end sensory epithelium is disorganized, and presynaptic ribbons are reduced in *Isl1CKO*. (**A**) The organ of Corti of *Isl1CKO* is shorter than control, as shown by anti-Myo7a labeling of hair cells in the cochlea at P0. **(B)** The length of the organ of Corti was measured at postnatal day P0 and in 2-month-old mice. Error bars represent mean ± SD; unpaired *t*-test. (**C**) Immunohistochemistry for prestin (a marker for OHCs) and calretinin (a marker for IHCs) shows a comparable cytoarchitecture of the organ of Corti in the cochlear mid-base of controls and *Isl1CKO* but disorganized rows of OHCs in the apical end with multiple OHC rows and ectopic calretinin$^{+}$ IHCs among OHCs (arrowheads) in *Isl1CKO* at P35. **(D)** Higher-magnification images show a detail of anti-tubulin labeled innervation with fibers forming three parallel outer spiral bundles (arrows) that innervate multiple OHCs and turn toward the base in the control cochlea. Guiding defects in the extension of these fibers to OHCs are obvious in *Isl1CKO* with some fibers randomly turned toward the apex (arrowheads); note the disorganization of radial fiber bundles in *Isl1CKO*. **(E)** Representative images of whole-mount immunolabeling of the cochlear mid-base with calretinin (IHCs) and anti-CtBP2 (presynaptic ribbons) of 2-month-old mice. **(F)** CtBP2$^{+}$ synapses were counted in 10 IHCs per each cochlear region (n = 6 mice per genotype). Box plots indicate median (middle line), 25th, 75th percentile (box) and min to max (whiskers); multiple *t*-tests, ****P < 0.000001. HS, Hoechst nuclear staining; IHC, inner hair cell; OHC, outer hair cell. Scale bars: 100 µm (A), 50 µm (C), 20 µm (D), 10 µm (E).

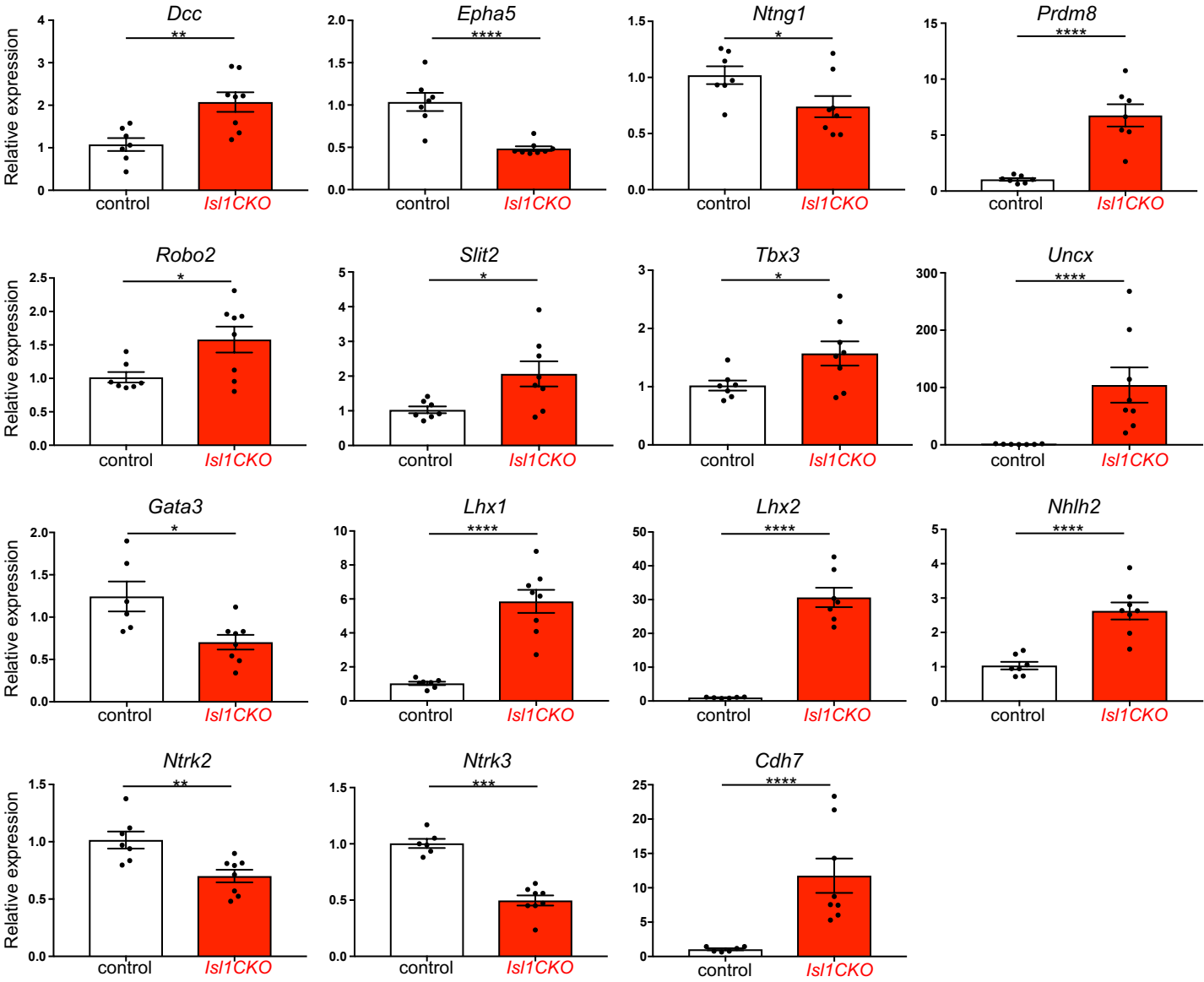


**Fig. S5. Validation of relative mRNA expression levels of selected genes by RT-qPCR.** RNA was isolated from the embryonic whole inner ear at E14.5. Data are normalized to *Hprt1* mRNA of the control gene. Data are expressed as mean ± SEM; unpaired *t*-test, *P < 0.05, **P < 0.01, ***P < 0.001, ****P < 0.0001. *Dcc*, deleted in colorectal carcinoma; *Epha5*, Eph receptor A5; *Ntng1*, netrin G1; *Prdm8*, PR domain containing 8; *Robo2*, roundabout guidance receptor 2; *Slit2*, slit guidance ligand 2; *Tbx3*, T-box 3; *Uncx*, UNC homeobox; *Gata3*, GATA binding protein 3; *Lhx1*, LIM homeobox protein 1; *Lhx2*, LIM homeobox protein 2; *Nhlh2*, nescient helix loop helix 2; *Ntrk2* and *Ntrk3*, neurotrophic tyrosine kinase receptors type 2 and type 3; and *Cdh7*, cadherin 7.

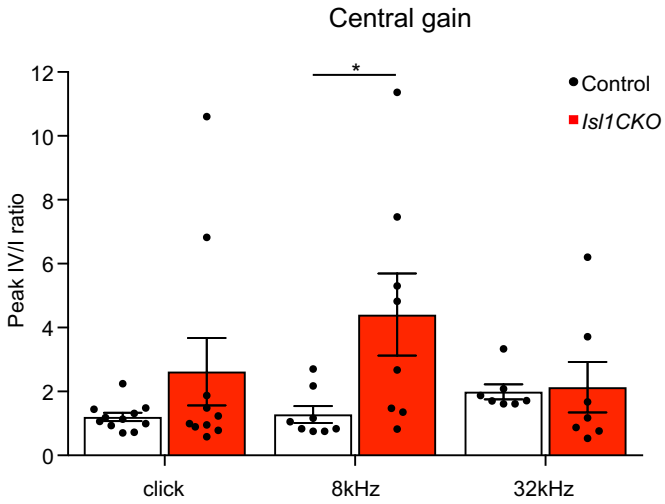


**Fig. S6. Average ratios of amplitudes of ABR peak IV relative to peak I.** Ratios are calculated for responses to clicks at stimulus levels of 80 dB SPL and tones of frequencies 8 and 32 kHz at stimulus levels of 90 dB SPL. Data are expressed as mean ± SEM. Two-way ANOVA with Bonferroni post hoc test, *P < 0.05.

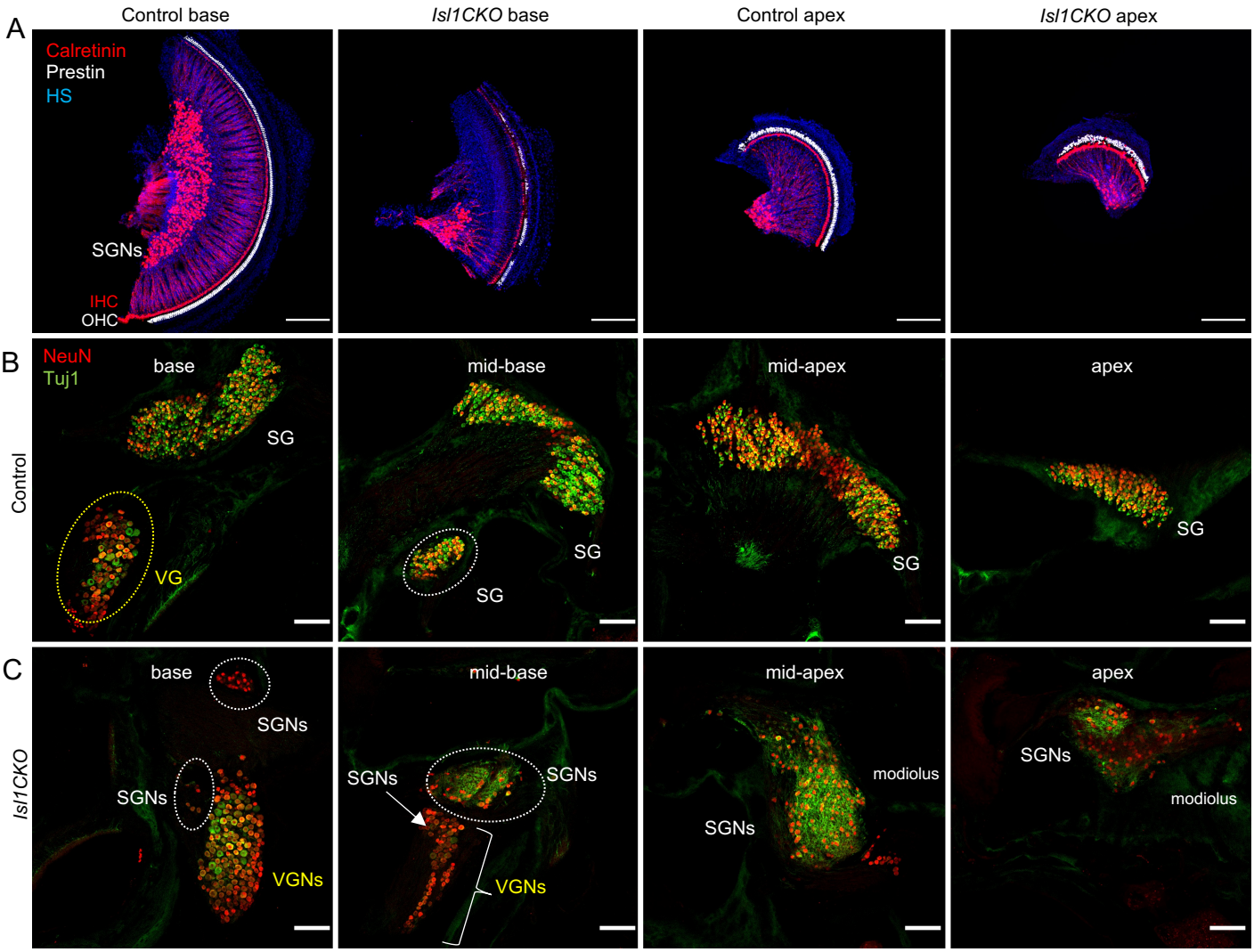


**Fig. S7. Adult neuronal phenotype of the inner ear. (A)** Anti-calretinin labeled inner hair cells (IHC) and SGNs type Ia are shown in cochlear whole mounts of 2-month-old mice. Anti-prestin labels outer hair cells (OHC) in the sensory epithelium. **(B)** Representative images of the control inner ear sections show the location of neurons in the SG in the Rosenthal's canal and in the VG of 2-month-old-mice. Four cochlear regions, the apex, mid-apex, mid-base and base, are shown. **(C)** SGNs are misplaced in the modiolus and mixed with VGNs, based on their soma size in the adult *Isl1CKO* inner ear. HS, Hoechst nuclear staining; SG, spiral ganglion; SGNs, spiral ganglion neurons; VGNs, vestibular ganglion neurons; VG, vestibular ganglion. Scale bars: 200 µm (A), 100 µm (B, C).

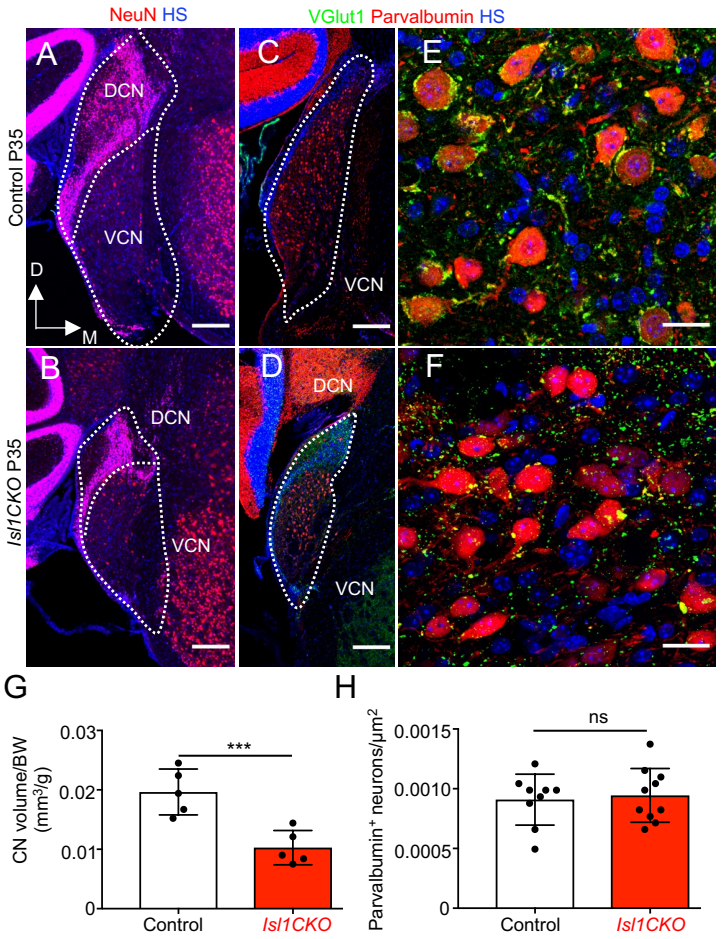


**Fig. S8. The cochlear nucleus of *Isl1CKO* is reduced. (A, B)** Coronal sections of a brain (immunostained with anti-NeuN) of adult controls and *Isl1CKO*, show the DCN and VCN; the dotted line indicates the boundaries of the CN. **(C-F)** Representative images of immunolabeled brain sections with anti-parvalbumin to label the spherical bushy cell soma and anti-VGlut1 to label auditory-nerve endbulbs of Held around the bushy cells. Higher-magnification images show the distribution of parvalbumin$^+$ neurons and the presence of VGlut1$^+$ auditory nerve synaptic terminals. (**G**) Quantification of the adult CN volume, adjusted to body weight (n = 5 mice per genotype) and **(H)** parvalbumin$^+$ neurons per µm$^2$ of the AVCN (n = 3 mice per genotype, 2-4 sections per mouse). Data are expressed as mean ± SD, unpaired *t-test* (***P < 0.001; ns, not significant). D, dorsal; M, medial axis; HS, Hoechst nuclear staining; DCN, dorsal cochlear nucleus; VCN, ventral cochlear nucleus. Scale bars: 200 µm (A-D); 20 µm (E,F).

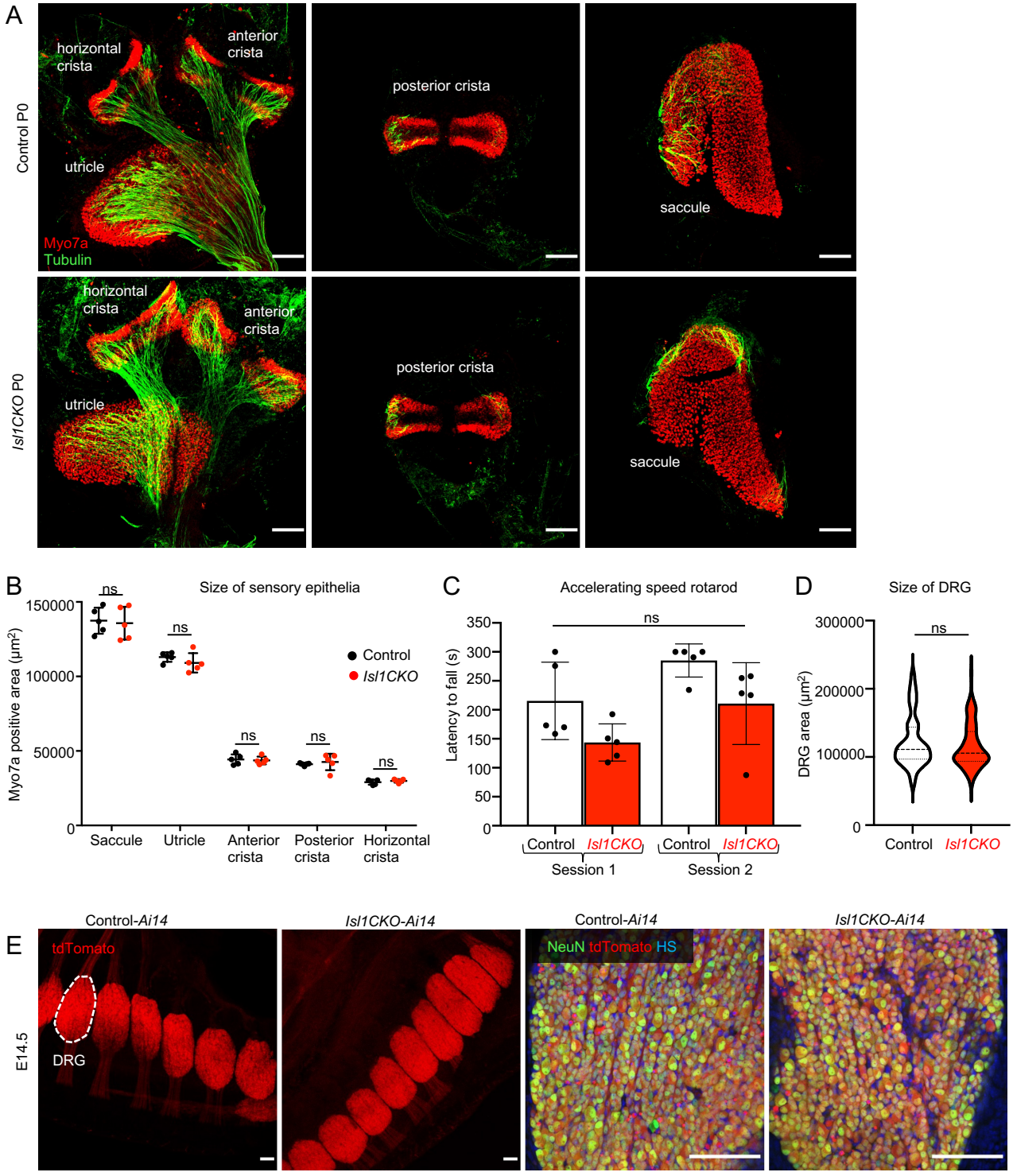


**Fig. S9. Vestibular function unaffected in *Isl1CKO*.** **(A)** Representative images of whole-mount immunolabeling of the vestibular-end organs with anti-Myo7a (a marker of hair cells) and anti-α-tubulin (nerve fibers) at P0. **(B)** The relative size of Myo7a positive sensory epithelia of the vestibular-end organs is comparable between control and *Isl1CKO* mice. Error bars represent mean ± SD (n = 5 mice per genotype), *t*-tests (P > 0.05, ns, not significant). **(C)** Motor coordination of *Isl1CKO* is comparable to control mice, as evaluated on the accelerating rotarod. Mice were tested in three consecutive trials in one session per day. Histograms represent the means of three trials per animal and 5 mice per genotype ± SD, repeated measures ANOVA (P = 0.055, ns, not significant). **(D)** The quantification of the DRG area (n = 6 embryos per genotype and two sections per embryo). Violin plots indicate median (middle line), 25th, and 75th percentile (dotted lines). Mann-Whitney *U* test (P = 0.304, ns, not significant) **(E)** Representative images of sagittal sections of E14.5 embryos show normal-sized dorsal root ganglia (DRG) in *Isl1CKO*. Higher-magnification images show NeuN (a marker of differentiated neurons) and tdTomato positive DRG neurons. HS, Hoechst nuclear staining. Scale bars: 100 µm.

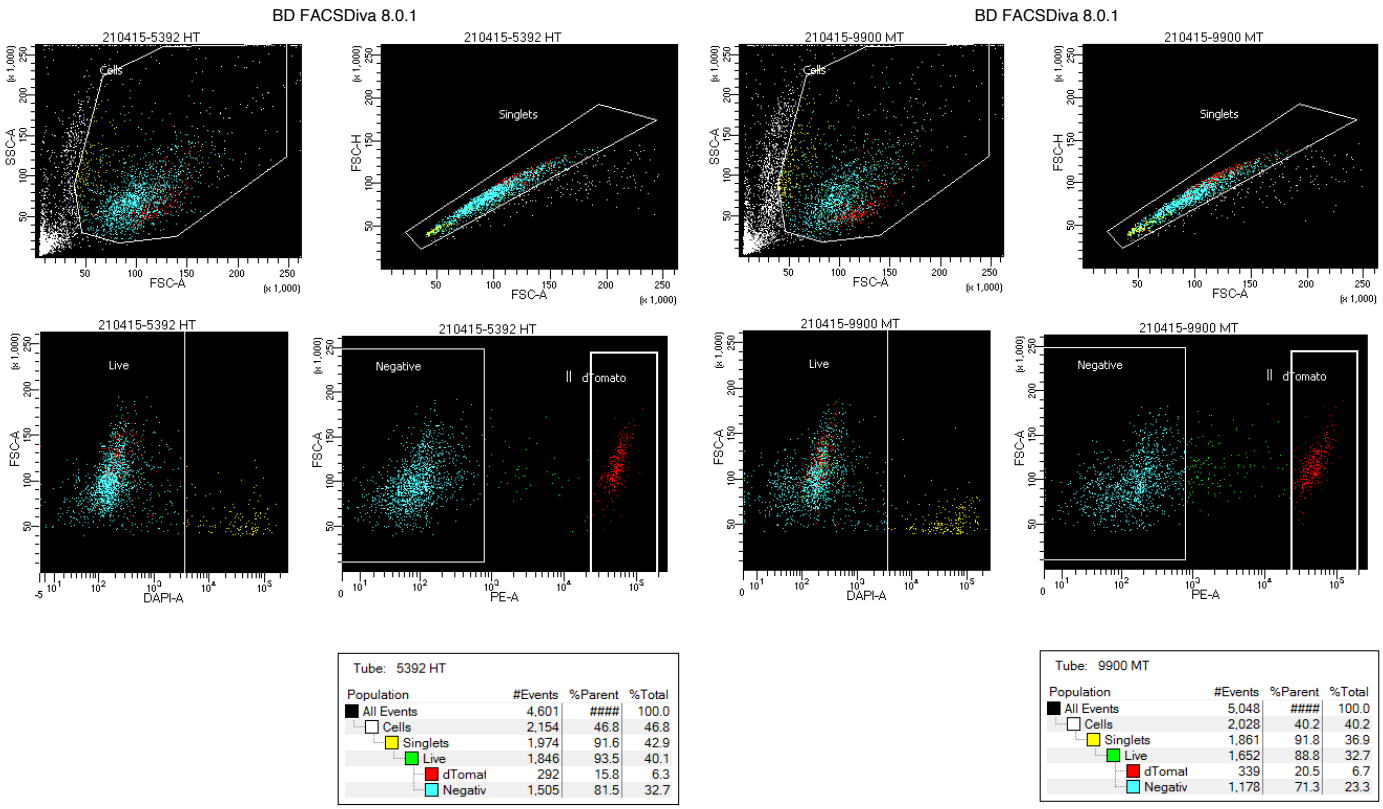


Tube: 5392 HT

| Population | #Events | %Parent | %Total |
|---|---|---|---|
| All Events | 4,601 | #### | 100.0 |
| Cells | 2,154 | 46.8 | 46.8 |
| Singlets | 1,974 | 91.6 | 42.9 |
| Live | 1,846 | 93.5 | 40.1 |
| dTomat | 292 | 15.8 | 6.3 |
| Negativ | 1,505 | 81.5 | 32.7 |

Tube: 9900 MT

| Population | #Events | %Parent | %Total |
|---|---|---|---|
| All Events | 5,048 | #### | 100.0 |
| Cells | 2,028 | 40.2 | 40.2 |
| Singlets | 1,861 | 91.8 | 36.9 |
| Live | 1,652 | 88.8 | 32.7 |
| dTomat | 339 | 20.5 | 6.7 |
| Negativ | 1,178 | 71.3 | 23.3 |

**Fig. S10. Gating strategy used to isolate tdTomato$^+$ cells.** Representative example to show gating to purify live and individual tdTomato$^+$ cells for RNAseq.

**Table S1.** Ribbon synapses (mean ± SD) per inner hair cell in the control and *Isl1CKO* cochlea of 2-month-old mice*

| Cochlear region | control | *Isl1CKO* |
|---|---|---|
| Base | 14.40 ± 3.346 | 6.57 ± 1.681 |
| Mid-base | 15.18 ± 3.154 | 7.54 ± 1.888 |
| Mid-apex | 13.65 ± 2.956 | 7.60 ± 2.618 |
| Apex | 11.04 ± 2.956 | 7.60 ± 2.068 |

*n = 6 cochlea per genotype/10 cells per each section (with the exception of only 5 samples of the apex in the control group)

## Table S2. Primer sequences for RT-qPCR

| Gene name | Forward | Reverse | Product size |
|---|---|---|---|
| *Lhx1* | CCCATCCTGGACCGTTTCC | CGCTTGGAGAGATGCCCTG | 193 bp |
| *Lhx2* | CGAGGGCTCACGAAGACCAT | AGCAGGTAGTAGCGGTCAGA | 95 bp |
| *Cdh7* | AGCCAAAACGAGTTATACACTGC | TCTTAACCGTTGTTGTGTCACTG | 101 bp |
| *Nhlh2* | CAGCGTGTCGGACCTAGAG | CCAGGTTGAAAGCCTCCAC | 188 bp |
| *Ntrk2* | CTGGGGCTTATGCCTGCTG | AGGCTCAGTACACCAAATCCTA | 100 bp |
| *Ntrk3* | CTGAGTGCTACAATCTAAGCCC | CACACCCCATAGAACTTGACAAT | 157 bp |
| *Dcc* | GCTATGGTGTTGGCAGTCCT | TAATCAACGGGGTCAGTGGG | 196 bp |
| *Epha5* | CTGGCGGACGGAAAGATGT | TTCAGGCCGATTTGCTGGG | 118 bp |
| *Gata3* | CCTCTACGCTCCTTGCTACTC | AGAGGAATCCGAGTGTGACC | 94 bp |
| *Ntng1* | CCAGTATCGGTACTAATGTCTGC | CCGTAGCTTCTCACAGAGGATG | 136 bp |
| *Prdm8* | AGAACGCCATATTCGGTCCC | ATTTGCCGCCGAAGTGTCTA | 131 bp |
| *Robo2* | GCTGAGAATCGGGTGGGAAA | AACTGTGGAGGAGCAACAGG | 77 bp |
| *Slit2* | CGAGAGTTTGTCTGCAGTGATG | CTACAGGTACAAGCAGCGGG | 95 bp |
| *Tbx3* | CAACTCTCGGTGGATGGTGG | TTGCGTGATCGCTTGGGAA | 188 bp |
| *Uncx* | ACCCGCACCAACTTTACCG | TGAACTCGGGACTCGACCA | 128 bp |
| *Hprt* | GCTTGCTGGTGAAAAGGACCTCTCGAAG | CCTGAAGTACTCATTATAGTCAAGGGCAT | 117 bp |

**Movie S1**_ Control cochlea_tdTomato_Myo7a_labeling
3D visualization of the control cochlea using light-sheet fluorescent microscopy. Neurons were visualized by tdTomato reporter expression and hair cells of the organ of Corti were immunolabeled using anti-Myo7a antibody. A part of the saccule with Myo7a positive hair cells is captured.

**Movie S2**_ Control cochlea_tdTomato_NeuN_labeling
3D visualization of the control cochlea using light-sheet fluorescent microscopy. Neurons were visualized by tdTomato reporter expression and by the immunolabeling of NeuN, a nuclear marker of differentiated neurons. TdTomato labeled projections are captured.

**Movie S3**_Isl1CKO cochlea_ tdTomato_Myo7a_labeling
3D visualization of the cochlea of Isl1CKO using light-sheet fluorescent microscopy. Neurons were visualized by tdTomato reporter expression and hair cells of the organ of Corti were immunolabeled using anti-Myo7a antibody. A part of the saccule with Myo7a positive hair cells is captured.

**Movie** S4_Isl1CKO cochlea_tdTomato_NeuN_labeling
3D visualization of the cochlea of Isl1CKO using light-sheet fluorescent microscopy. Neurons were visualized by tdTomato reporter expression and by the immunolabeling of NeuN, a nuclear marker of differentiated neurons.